ACS OMEGA

http://pubs.acs.org/journal/acsodf

Article

Kinetics and Thermodynamics of Hemicellulose Adsorption onto Nanofibril Cellulose Surfaces by QCM-D

Mingzhu Yao, Chen Liang, Shuangquan Yao, Yang Liu,* Hui Zhao, and Chenni Qin

Cite This: *ACS Omega* 2021, 6, 30618−30626

Read Online

ACCESS | Metrics & More | Article Recommendations

ABSTRACT: The adsorption of hemicellulose derived from bagasse onto nanofibril cellulose has been studied in terms of kinetics and thermodynamics. In situ monitoring of bagasse hemicellulose with different molecular weights onto the nanofibril cellulose surfaces has been investigated using quartz crystal microbalance and dissipation. Then, the adsorption kinetics and thermodynamic properties were analyzed. Also, the sorption behavior and the adsorption layer properties were quantified in aqueous solutions. The maximum adsorption mass was 2.8314 mg/m^2 at a concentration of 200 mg/L. Also, compared with that of the low-molecular-weight hemicellulose, the adsorption capacity of the high-molecular-weight hemicellulose was higher, and the adsorption rate changed faster and could reach an equilibrium in a shorter time. The intraparticle diffusion kinetic model represented the experimental data very well. Therefore, the kinetics of hemicellulose on the fiber adsorption was commonly described by a three-stage process: mass to transfer, diffusion, and equilibrium. The Gibbs energy change of the adsorption of hemicellulose was found to range from −20.04 to −49.75 kJ/mol at 25 °C. The entropy change was >0. It was found that the adsorption was spontaneous, and the adsorbed mass increased with the increase in temperature. This strengthened the conclusion that the adsorption process of the bagasse hemicellulose on the NFC was driven by the increase in entropy caused by the release of water molecules due to hydrophobic interaction or solvent reorganization.

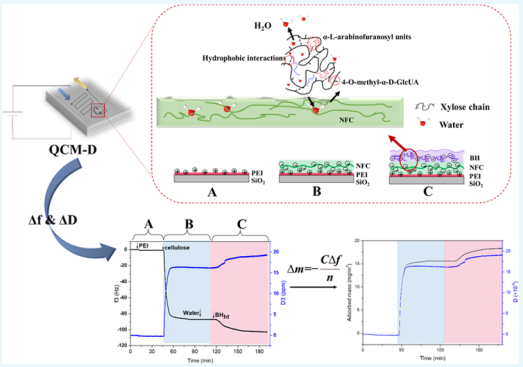

1. INTRODUCTION

Cellulose material has become a research hotspot in recent years[1−3] because it is the most abundant renewable material on the planet.[4,5] As a substitute for petroleum-derived materials, cellulose is widely used in many industries such as papermaking,[3] packaging, and building materials.[2] However, hemicellulose is often discarded as biomass waste during the industrial processing of plant fibers. It is a type of natural polymer with a high molecular weight, the second-highest after cellulose, which was a general term for a class of heterogeneous polysaccharides, including xylose, galactose, arabinose, mannose, and so on.[6] Hemicellulose acts as a binder in plant cell walls. The study of the interaction between hemicellulose and cellulose plays an important role in fiber assembling and the role of amorphous polymers in shaping the structure of the fiber network.[7−9] Some studies have shown that the blend of oligosaccharides and polysaccharides with cellulose had excellent hydrophobicity and barrier properties. The application and development of hemicellulose could be used to prepare high-value materials, such as oxygen barrier films for packaging, plastic adhesives, and improvement of paper strength in the paper industry.[10] Therefore, it is important to reveal the interaction between hemicellulose and cellulose.[11−13]

In recent years, some researchers have used molecular dynamics simulation and atomic force microscopy to study the interaction. However, molecular simulations could not handle complex systems, and processes occurring in large spaces and in long timescales in the methods of atomic force microscopy can only study the frictional force of polysaccharides on the surface of cellulose on a macro scale.[14,15] At present, some researchers also used a microcrystalline quartz balance with dissipation to study the interaction between xylan and cellulose. Jaafar et al.[16] proved that acetylated xylan formed a dense rigid layer on the cellulose. Bosmans et al.[17] quantitatively studied the adsorption of debranched xylan on the surface of the cellulose. Köhnke et al.[18] proved that the hydrodynamic properties of arabinoxylan depend not only on the degree of substitution but also on the substitution mode. Due to the complex molecular structure and different molecular weights of the hemicellulose, there was no evidence

Received: August 14, 2021
Accepted: October 20, 2021
Published: November 4, 2021

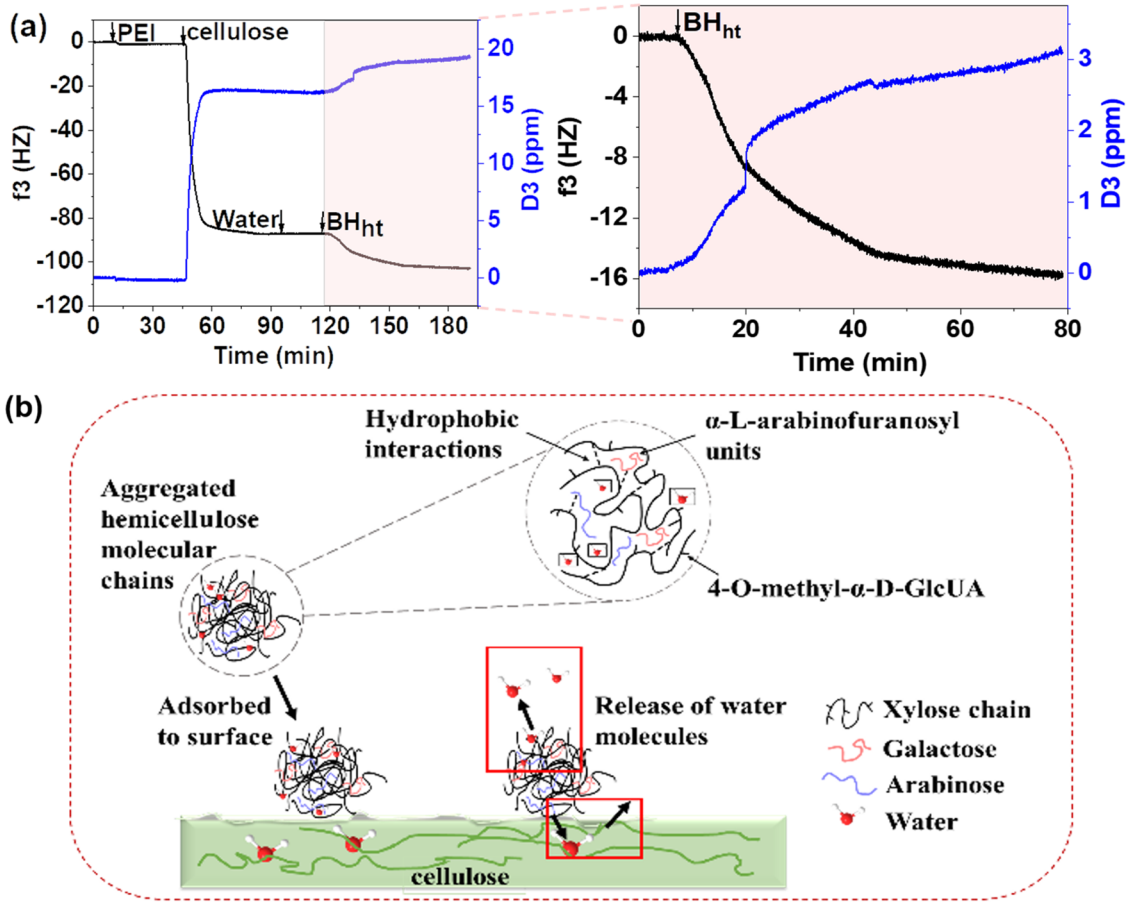

Figure 1. PEI, NFC, and BH_{ht} adsorbed on the SiO_2 surface through a layer-by-layer assembly process and the mechanism diagram. (a) Frequency (f3) and dissipation under the third overtone (D3) in the layer-by-layer assembly process and (b) mechanism diagram of the adsorption process.

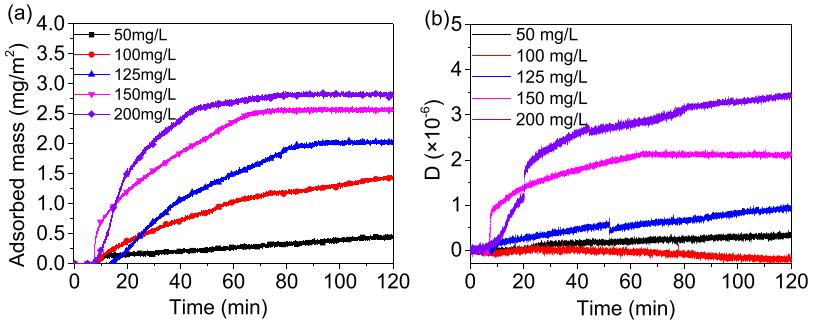

Figure 2. Adsorption capacity (a) and dissipation curve (b) of BH_{ht} on NFC was measured at different concentrations (50, 100, 125, 150, 175, 200 mg/L), 25 °C, f = 5 MHz, n = 3, pH = 7, and a flow rate of 100 μL/min.

of the mechanism of this interaction, adsorbed kinetic behavior, and thermodynamics. The main factors controlling the adsorption of cellulose by hemicellulose needed to be further clarified and studied.

In this study, the objective was to investigate the hemicellulose of different molecular weights obtained by this approach from bagasse by in situ monitoring the adsorbed kinetic behavior on cellulose nanofiber (NFC) surface using quartz crystal microbalance with dissipation (QCM-D). Thermodynamic and kinetic parameters of the adsorption of hemicellulose of different molecular weights onto a cellulose nanofiber surface were determined to evaluate enthalpic effects related to interactions and the adsorption kinetic behavior. The study revealed the hemicellulose−cellulose interaction and provided directions for the design and optimization of materials based on eco-friendly polysaccharides to render biomass materials more amenable to processing.

2. RESULTS AND DISCUSSION

2.1. Adsorption of Hemicellulose onto NFC Surfaces.

The adsorption of hemicellulose from bagasse on the surface of cellulose was studied using QCM-D. By measuring the change in resonance frequency caused by adsorption, the adsorption kinetic process was measured in real time. Using eq 1, the frequency change was translated into the adsorption mass, as shown in Figure 1. Three stepwise increments in the frequency could be observed, which was the adsorption of PEI, which had been used for facilitating cellulose adsorptive on the silicon

https://doi.org/10.1021/acsomega.1c04391
ACS Omega 2021, 6, 30618−30626

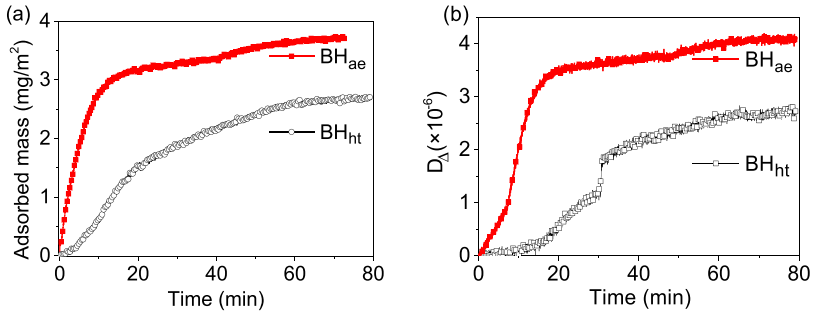

Figure 3. Adsorption capacity (a) and dissipation curve (b) of BH_{ht} and BH_{ae} on NFC was measured at 25 °C, f = 5 MHz, n = 3, pH = 7, concentration of 150 mg/L, and a flow rate of 100 μL /min.

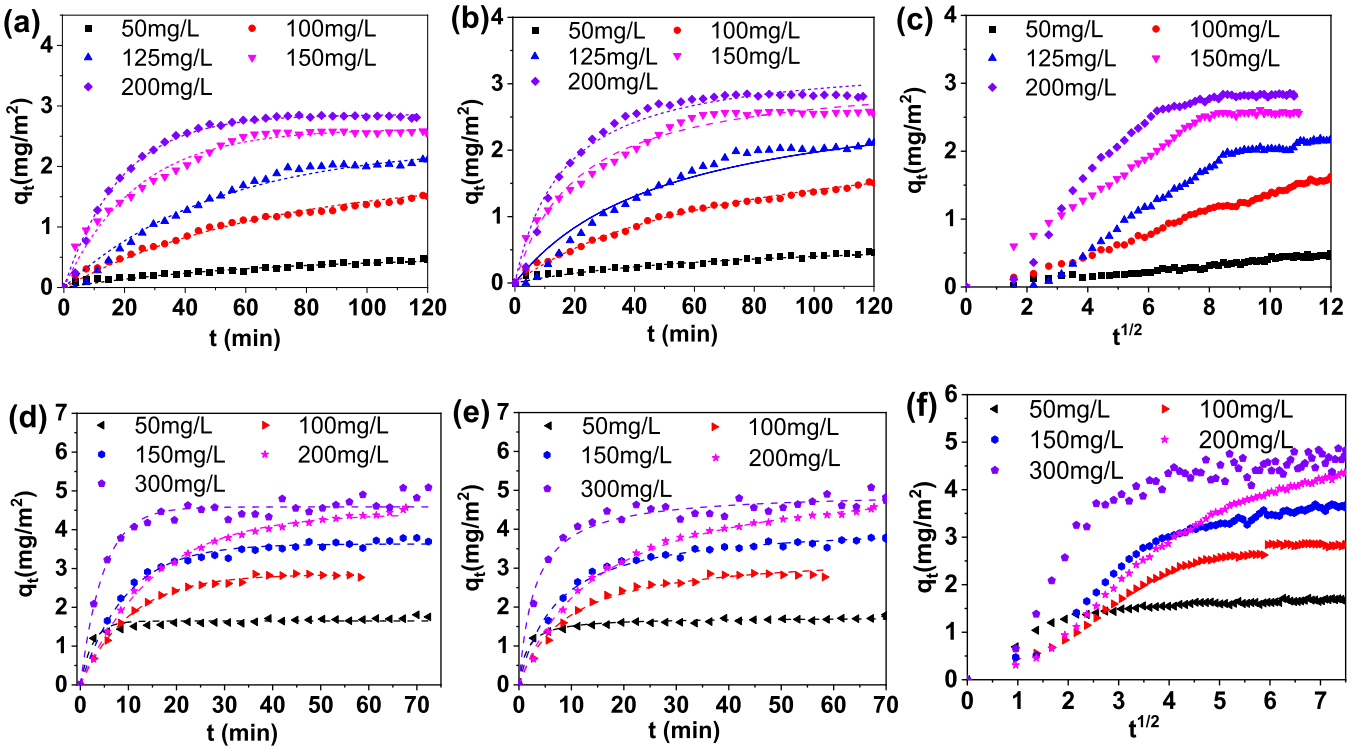

Figure 4. Pseudo-first-order (a, d), pseudo-second-order (b, e), and intraparticle diffusion kinetic model; (c, f) plots for BH_{ht} and BH_{ae} adsorption on NFC at different concentrations at 25 °C, f = 5 MHz, n = 3, pH = 7, and a flow rate of 100 μL/min. The points were the experimental data, and the dashed lines were the fitting results.

sensor, the adsorption of NFC, and the adsorption of BH_{ht}. When the NFC reaches an adsorption mass of **15.5801 mg/m²**, the adsorption is saturated, and there is no obvious desorption phenomenon after Milli-Q water washing, which indicates that NFC had completely covered the SiO_2 chip to form a uniform film. The adsorption mass of BH_{ht} was **2.7940 mg/m²** (Figure 2). When the frequency decreased, the dissipation gradually increased in the same trend. Thus, the NFC formed a uniform and soft thin layer on the surface of SiO_2. The adsorption curve of BH_{ht} gradually achieved an equilibrium after 60 min. This study assumes that the adsorption process of hemicellulose on NFC is spontaneous and driven by the increase in entropy caused by the release of water molecules due to hydrophobic interaction or solvent reorganization.[19,20] The hemicellulose entered the cellulose pores and released some of the surrounding water molecules (Figure 1c).

To find the best concentration for studying the adsorption behavior, different concentrations of BH_{ht} were tested. When BH_{ht} was injected into the flow cell in the given concentrations (50, 100, 125, 150, 200 mg/L) at 25 °C, the adsorption capacity and dissipation of BH_{ht} on the NFC changed as shown in Figure 2. When the concentration was increased from 50 to 200 mg/L, the adsorption capacity increased from 0.4505 to 2.8314 mg/m². However, when the concentration was 200 mg/L, the adsorption process was extremely unstable and desorption occurred. When the concentration was 150 mg/L, the adsorption capacity was the same at about 2.5545 mg/m². Therefore, the concentration of 150 mg/L was selected as the experimental concentration for the following study.

2.2. Influence of the Molecular Weight of Hemicellulose. The adsorption process of BH_{ht} and BH_{ae} at a concentration of 150 mg/L on cellulose was studied by the layer-by-layer assembly at 25 °C. Compared with the adsorption capacity of low-molecular-weight hemicellulose, that of the high-molecular-weight hemicellulose was higher and the adsorption rate changed faster and could reach equilibrium in a shorter time. This was because the hemicellulose BH_{ae}

https://doi.org/10.1021/acsomega.1c04391
ACS Omega 2021, 6, 30618−30626

with a large molecular weight was loosely bound to the cellulose surface, and the movable polymer segments moved together with the adsorbed water during the shaking and shearing processes, resulting in an increase in adsorption capacity.[21] According to the molecular entanglement theory, the higher the molecular weight, the more entangled the molecular chains are and more adsorbed water between the molecules, resulting in a higher adsorption capacity and a higher dissipation value.[22,23] BH_{ht} was tightly bound on the surface of cellulose, less adsorbed water moved with the shear layer, and the dissipation was lower. Thereby, compared with the absorption of BH_{ae}, the formed adsorption layer of BH_{ht} had stronger rigidity and binding force (Figure 3).

2.3. Sorption of Bagasse Hemicellulose Kinetics. To better illustrate the adsorption behavior and the adsorption kinetics of BH_{ht} and BH_{ae}, the pseudo-first-order, pseudo-second-order, and intraparticle diffusion kinetics were exercised to fit the adsorption data at different concentrations.

The pseudo-first-order kinetic equation is given by

$$q_t = q_e[1 - \exp(-k_1 t)] \quad (1)$$

The pseudo-second-order kinetic equation is given by

$$q_t = \frac{k_2 q_e^{\ 2} t}{1 + q_e k_2 t} \quad (2)$$

where k_1 is the pseudo-first-order rate constant (1/min). q_t is the amount of adsorption at a given point in time, k_2 is the pseudo-second-order rate constant ($m^2/(mg{\cdot}min)$), t is the time elapsed from the beginning of the adsorption process, and q_e is the amount adsorbed at equilibrium. The intraparticle diffusion kinetic equation is

$$q_t = k_p \times t^{1/2} + C \quad (3)$$

where k_p is the intraparticle diffusion order rate constant ($mg{\cdot}m^{-2}{\cdot}min^{1/2}$) and C is the intercept distance. The kinetic curve of the intraparticle diffusion could be divided into three parts: fast adsorption stage, diffusion stage, and adsorption equilibrium stage.

Figure 4 shows BH_{ht} and BH_{ae} adsorbed mass vs time at different concentrations, as well as the fitting curves of pseudo-first-order (a, d), pseudo-second-order (b, e), and intraparticle diffusion models (c, f), whereas the kinetic parameters and correlation coefficients are shown in Table 1. It can be observed that the adsorption kinetics do not fit the pseudo-first-order and pseudo-second-order model well with $R^2 < 0.95$ at BH_{ht} concentrations of 50 mg/L and BH_{ae} concentrations of 300 mg/L. Also, the adsorption kinetics did not fit the pseudo-first-order model at BH_{ae} concentrations of 50 mg/L. The experimental data points differ markedly from the linear adjustment curve at the adsorption equilibrium stage, and the equilibrium adsorption mass (q_e) was also markedly higher than the experimental value (Table 1). The results indicate that when the hemicellulose concentration was too high or too low, the pseudo-first-order and the pseudo-second-order kinetic model could not fit the adsorption process well.

Figure 4c,f shows that eq 3 fits well with the experimental data for BH_{ht} and BH_{ae} adsorption on NFC. The kinetics of hemicellulose on the fiber adsorption was commonly described by a three-stage process.[24] The R^2 for the three-stage process in Table 1 was in the range of 0.95−0.99. The first stage was the diffusion of hemicellulose molecules on the fiber surface, which

Table 1. Kinetic Models and Fitting Parameters for Bh_{ht} and Bh_{ae} Adsorption on NFC at Different Concentrations

model		BH_{ht}						BH_{ae}					
	C_0 (mg/L)	50	100	125	150	200		50	100	150	200	300	
experiment	q_e (exp)(mg/m^2)	0.457	1.673	2.59	2.26	2.833		1.758	2.86	3.77	4.47	4.79	
pseudo-first-order	q_e (fit)	0.5122	1.838	2.3456	2.6238	2.8582		1.647	2.846	3.632	4.418	4.587	
	k_1	0.0156	0.0149	0.0199	0.0416	0.0535		0.399	0.096	0.106	0.065	0.209	
	adj. R^2	0.9373	0.9913	0.9865	0.9736	0.9915		0.873	0.933	0.985	0.996	0.932	
pseudo-second-order	q_e (fit)	0.6985	2.4123	2.9738	3.1617	3.3885		1.731	3.405	4.1503	4.472	4.9662	
	k_2	0.0191	0.0057	0.0066	0.0152	0.0185		0.3935	0.0328	0.0343	5.5107	0.06558	
	adj. R^2	0.9521	0.997	0.974	0.9742	0.9679		0.9624	0.9853	0.9837	0.9959	0.9574	
intraparticle diffusion kinetic model	K_{p1}	0.1564	0.1519	0.3111	0.3119	0.5308		1.5571	0.6679	1.0165	0.9045	1.9176	
	adj. R_1^2	0.9932	0.9951	0.9958	0.9979	0.9889		0.9774	0.9911	0.9918	0.9918	0.9718	
	K_{p2}	0.0411	0.10231	0.0908	0.0817	0.09683		0.3795	0.1704	0.3349	0.3375	0.3688	
	adj. R_2^2	0.9592	0.9506	0.9952	0.9572	0.9957		0.9506	0.9894	0.9562	0.9691	0.9552	
	K_{p3}	0.0089	0.0791	0.0127	0.00281	0.00215		0.0445	0.0519	0.1317	0.2332	0.1262	
	adj. R_3^2	0.9521	0.9595	00.9961	0.9772	0.9564		0.9551	0.9506	0.9717	0.9562	0.9691	

https://doi.org/10.1021/acsomega.1c04391
ACS Omega 2021, 6, 30618−30626

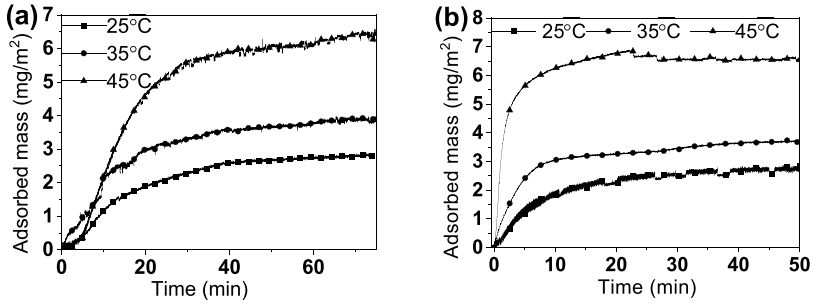

Figure 5. Hemicellulose adsorption capacity curves at different temperatures (25, 35, 45 °C), f = 5 MHz, n = 3, pH = 7, a concentration of 150 mg/L, and a flow rate of 100 μL/min ((a) BH_{ht} adsorption capacity curve and (b) BH_{ae} adsorption capacity curve).

was the phenomenon of the mass transfer due to the random thermal motion of molecules under the condition that there was a difference in concentration within a phase. In the second stage, some of the hemicellulose was diffused into the fiber pores after a certain amount of it was adsorbed on the fiber. Eventually, as the diffusion of hemicellulose to the fiber surface and pores increased, the adsorption gradually reached a steady state.[25]

2.4. Thermodynamics of Bagasse Hemicellulose Adsorption. The adsorption capacity of BH_{ht} and BH_{ae} on NFC at different temperatures is shown in Figure 5. As the temperature increased, the adsorption capacity increased. According to Figure 5a, the adsorption masses of BH_{ht} and BH_{ae} are 2.76 and 2.67 mg/m^2 at 25 °C, respectively. When the temperature increased to 45 °C, the adsorption masses were 6.43 and 6.61 mg/m^2, respectively, and the adsorption mass increased by 57−59%. However, when the temperature was 45 °C, after BH_{ht} and BH_{ae} reached the maximum adsorption capacity, the adsorption capacity fluctuated slightly after 20 min. This could be due to the formation of the first layer of hemicellulose at the cellulose surface by hydrogen bonding during the adsorption process.[26,27] After the monomer was diffused on the cellulose surface, it formed a second layer of accumulation.[28,29] Compared with the first adsorption layer, the second layer had a weaker hydrogen bond force and a smaller proportion, so the adsorption layer was extremely unstable, and there was some desorption after the equilibrium-related phenomenon. It was proved that the main binding site was controlled by hydrogen bonds in hemicellulose and cellulose. It was found from the cellulose X-ray structure that the interaction was hydrophobic and the intermolecular C−H···O interactions were weak in the second layer of accumulation. This was consistent with the research conclusion of Silveira et al.,[15] who used the 3D-RISM-KH molecular solvation theory to explain the phenomenon.

This temperature effect can also be demonstrated through the Gibbs energy change (ΔG), which could be computed as follows

$$\Delta G = -RT \ln K_a \tag{4}$$

where R (8.314 J/(mol·K)) is the gas constant, T is the absolute temperature in kelvin, and K_a is the adsorbed mass at different temperatures.[23]

The van't Hoff equation was used to analyze the standard entropy change (ΔS) and enthalpy change (ΔH) of BH_{ht} and BH_{ae} at different temperatures[30]

$$\ln K_a = -\frac{\Delta H}{RT} + \frac{\Delta S}{R} \tag{5}$$

where the corresponding ΔH and ΔS were assessed by a plot of $\ln K_a$ versus $1/T$, which yields a straight line with an intercept of $\Delta S/R$ and a slope of $-\Delta H/R$. Figure 6 shows the van't Hoff plot for the determination of the thermodynamic parameters that are presented in Table 2.

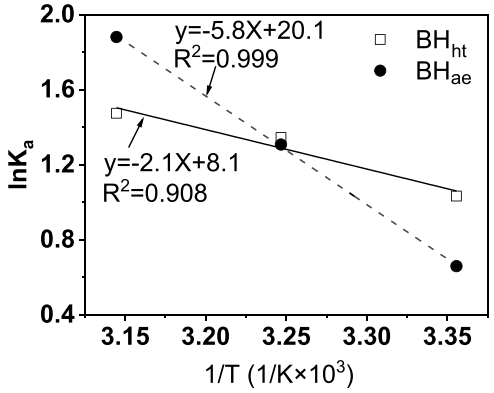

Figure 6. van't Hoff curves and regression analysis.

Table 2. Thermodynamic Parameters of Bh_{ht} and Bh_{ae} Adsorption on NFC at Different Temperatures

hemicellulose	temp (°C)	ΔG (kJ/mol)	ΔH (kJ/mol)	ΔS (kJ/K·mol)
BH_{ht}	25	−20.0379		
	35	−20.7109	0.0175	0.0673
	45	−21.3839		
	25	−49.7476		
BH_{ae}	35	−51.4186	0.0482	0.1671
	45	−53.0896		

The relationship between ΔG, ΔH, and ΔS could be computed as follows

$$\Delta G = \Delta H - T\Delta S \tag{6}$$

According to Table 2, ΔG was negative during the adsorption of BH_{ht} and BH_{ae}, indicating that the adsorption was spontaneous. The enthalpy value was greater than zero, that is $\Delta H > 0$, indicating that the adsorption process of BH_{ht} and BH_{ae} on the cellulose surface was an endothermic reaction. The ΔG of BH_{ht} was in the range of −20.04 to −21.38 kJ/mol, indicating that the BH_{ht} adsorption process was a physical adsorption process dominated by van der Waals forces. ΔG was in the range of −49.74 to −53.09 kJ/mol during the adsorption of BH_{ae}. As it is known that the hydrogen bond energy was in the range of 8−50 kJ/mol, it can be observed that the hydrogen bond played a dominant role when BH_{ae} was

https://doi.org/10.1021/acsomega.1c04391
ACS Omega 2021, 6, 30618−30626

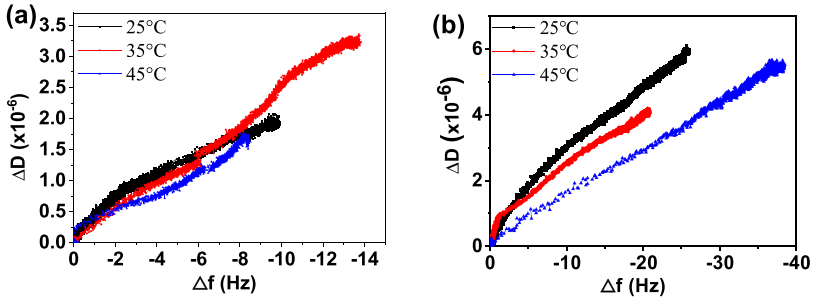

Figure 7. Plots of energy dissipation against frequency shift for the adsorption of (a) BH_{ht} and (b) BH_{ae} on NFC films (f = 5 MHz, n = 3).

adsorbed on the NFC. After the temperature increased, the interaction efficiency of hydrogen bond and van der Waals force was reduced.[23,25] Therefore, at temperatures higher than 45 °C, the adsorption process of BH_{ht} and BH_{ae} on NFC was driven by the increase in entropy caused by the release of water molecules due to hydrophobic interaction or solvent reorganization. The hemicellulose entered the cellulose pores and released some of the surrounding water molecules.[31] The soft conformation of the adsorption layer and the disorder of the cellulose chain led to an increase in entropy, and the adsorption process was sensitive to temperature. The first hydrogen bond site adsorbed was an exothermic behavior. Adsorption to the second position was the entropy-driven effect of heat absorption. With an increase in temperature, the hydrophobic interaction increased, and the amount of hemicellulose adsorption increased with the increase in temperature. This research result was consistent with the conclusion of Lopez et al.[32] that xyloglucan interacts with cellulose through two different processes as confirmed by the isothermal titration calorimetry (ITC) measurement.

2.5. Different Molecular Weights of Hemicellulose Affect the Properties of the Adsorbed Layer. The characteristics of the adsorption layer were qualitatively explored through the $\Delta D-\Delta f$ function relationship. The adsorption data points of BH_{ht} and BH_{ae} on NFC form a continuous curve, indicating that the adsorption of hemicellulose on NFC was a rather slow one. As the frequency decreased, the adsorption slope decreased slowly, and the adsorption layer changed from a looser layer to a tighter, harder, and less water-absorbing thin layer (Figure 7a). When Δf was less than −2 Hz, the temperature had a significant effect on the adsorption of BH_{ht} on the NFC surface, and the conformation of the adsorption layer was slightly changed and rearranged. When Δf was −2 to −6 Hz, the slope of the curve had a discontinuity point, which was due to the conformation of the adsorption layer changed again during the adsorption process.[33,34] The result indicated that the later adsorption was a sedimentary adsorption process. With the accumulation of hemicellulose molecules, steric hindrance and binding were observed. With the reduction of sites, the newly adsorbed hemicellulose molecules would remain on and around the cellulose surface, resulting in an increase in the dissipation value. The conformation of the adsorption layer undergoes a rearrangement at 25 °C. One stage formed a soft layer and then a compact layer, and the rearrangement was changed from a soft layer to a more rigid adsorption layer.

The viscoelastic properties of the high-molecular-weight BH_{ae} adsorption layer are shown in Figure 7b. Compared with the adsorption process of low molecular weight, the $\Delta D-\Delta f$ curve had a constant slope, indicating that the adsorption layer did not undergo a conformational change in response to the increase in the amount of adsorption during the BH_{ae} adsorption process.[18] As the adsorption temperature increases, the slope of the $\Delta D-\Delta f$ curve decreases significantly. Therefore, the higher the temperature, the harder the adsorption layer formed by BH_{ae} on the cellulose surfaces during the adsorption process. Compared with the low-molecular-weight hemicellulose, high-molecular-weight hemicellulose was more sensitive to temperature and not prone to conformational changes during adsorption.

The thickness (h), viscosity (η), and shear modulus (μ) of the adsorption film were quantitatively analyzed by QCM-D. The viscoelastic properties of the hemicellulose adsorbed layer were fitted by the Voigt model through the frequency and dissipation changes of several overtones. Since QCM-D could be used to monitor the quality of adsorbed water at the same time, the measured value had no practical significance. However, the results could be compared relative to each other.[35] When the temperature increased from 25 to 45 °C, the viscosity of BH_{ae} and BH_{ht} did not change significantly within the range of 1.0−1.4 Pa·s. The elastic modulus of BH_{ht} decreased from 81.79 to 6.64 kPa. The elastic modulus of BH_{ae} decreased from 8.5 to 4.4 kPa. However, the thickness of BH_{ht} increased from 1.64 to 4.86 nm. The BH_{ae} thickness did not change significantly. This was consistent with the conclusion in Figure 7. With the increase in temperature, the adsorption layer became looser and softer. This suggested that the creep resistance decreased when the temperature increased. This was consistent with the $\Delta D-\Delta f$ image analysis. The hemicellulose was assembled on the cellulose surface to form a relatively soft and loose adsorption layer. At 45 °C, the thickness of BH_{ae} was reduced to 2.74 nm and the thermal movement of water molecules was intensified, which enhanced the hydration state of xylan macromolecules.[9,36] Therefore, temperature not only affected the adsorption kinetics and adsorption capacity but also had a certain effect on the structure and properties of the adsorption layer. This research result was consistent with the conclusion of Pereira et al.[37] (Table 3).

2.6. Morphology after Adsorption on a Cellulose Layer. AFM was used to evaluate the morphology of the SiO_2 chip with NFC before and after hemicellulose adsorption. As shown in Figure 8a, a homogeneous distribution of nanofibrils can be seen all over the image area before hemicellulose adsorption. The SiO_2 chip was almost completely covered by the randomly oriented NFC, and the Ra was determined to be 14.3 nm. After the adsorption of hemicellulose on NFC, obvious changes could be seen, as shown in Figure 8b,c; the Ra was determined to be 13.4 nm. Figure 8c is a partially enlarged view of Figure 8b with the scanned surface of 200 × 200 nm^2

https://doi.org/10.1021/acsomega.1c04391
ACS Omega 2021, 6, 30618−30626

Table 3. Simulated Mean Shear h, μ, and η of the Hemicellulose Adsorbed Layers during the Adsorption Equilibrium Stage (t = 50−80 min)

	T (°C)	μ (KPa)	η (Pa·s)	h (nm)
BH_{ht}	25	81.79 ± 15.73	1.43 ± 0.49	1.6470 ± 1.27
	35	15.12 ± 0.07	1.22 ± 0.32	3.0867 ± 0.77
	45	6.64 ± 1.15	1.09 ± 0.14	4.8670 ± 1.69
BH_{ae}	25	8.50 ± 4.75	1.33 ± 0.23	3.0770 ± 1.27
	35	6.83 ± 0.95	1.21 ± 0.01	3.4070 ± 0.51
	45	4.44 ± 1.15	1.46 ± 0.57	2.7430 ± 1.02

and the height scale of 40 nm. The granular hemicellulose molecules could not be clearly seen in the image, but the pores between the cellulose and the fibers were filled and the cellulose fiber surface became smooth. This is because the hemicellulose was likely to present as a monolayer on the NFC surface and was deposited onto the cellulose fibrils (Figure 8c).

3. CONCLUSIONS

In the study, the detailed kinetic study of the adsorption of the BH of different molecular weights on the NFC surface led to the understanding of the effect of the interactions of cellulose with hemicellulose and the characteristics of the adsorbed layer. The adsorption kinetics did not fit the pseudo-first- and pseudo-second-order models well when the BH concentrations were less than 50 mg/L and more than 300 mg/L, whereas the intraparticle diffusion kinetic model fitted well with the experimental data for BH adsorption on NFC. Thus, the kinetics of hemicellulose on fiber adsorption was commonly described by a three-step process: mass transfer, diffusion, and equilibrium. Adsorption of high-molecular-weight hemicellulose on the NFC resulted in an excellent gain in the adsorption capacity and adsorption rate, while the equilibrium time was drastically reduced. Further, with the increase in temperature, the adsorbed mass increased, resulting in an endothermic reaction. Although a continuous enhancement and gain in the adsorbed mass were observed, the adsorbed layer was extremely unstable at 45 °C. This strengthened the conclusion that the adsorption process of bagasse hemicellulose on NFC was driven by the increased entropy caused by the release of water molecules due to hydrophobic interaction or solvent reorganization. These results gave a better understanding of the material of hemicellulose−cellulose interaction with the aim of encouraging the design of new biomimetic materials.

4. MATERIALS AND METHODS

4.1. Materials. Bleached sugarcane bagasse pulp was procured from Guangxi Guitang (China) Co., Ltd. Hemicellulose prepared by hydrothermal method (BH_{ht}, M_w = 25 202 g·mol^{-1}) and hemicellulose prepared by alkaline extraction (BH_{ae}, M_w = 66 500 g·mol^{-1}) were from Guangxi Key Laboratory of Clean Pulp & Papermaking and Pollution Control. Polyethylenimine (PEI) with M_w = 70 000 g·mol^{-1} and sodium dodecyl sulfate (SDS) were kindly supplied by Aladdin Reagent Co., Ltd. (China).

4.2. Preparation of Nanofibril Cellulose Substrate. The nanofibril cellulose was prepared by a high-consistency refiner, and 2.63 wt % of fibril pulp of 3.82 g was dispersed in 100 mL of Milli-Q water. The fibrillated cellulose suspension was dispersed by an ultrasonic probe (25% amplitude transformer, 20% power) for 7 min. Also, the dispersed fibrillated cellulose was centrifuged at 8000 rpm/min for 15 min and the supernatant was extracted. The carbohydrate composition of the nanofibrillated cellulose (NFC) was 77.56 wt % glucose and 22.43 wt % xylose.

4.3. QCM-D Experiments. QCM-D was used to monitor the adsorption kinetics of hemicellulose on the NFC film. The quartz crystal sensor chip (SiO_2 chip, QSX 303) was placed in the flow cell, and PEI (0.1 g·L^{-1}) was continuously injected into the flow cell at a constant temperature (25, 35, 45 °C) at a flow rate of 100 μL·min^{-1}. To promote the adhesion of NFC (1 g·L^{-1}) on the SiO_2 chip, when NFC adsorption reached equilibrium, it was washed with Milli-Q water to remove loosely adsorbed substances, and then, hemicellulose was introduced on the system of NFC. After each addition of attached substances, the mixture was rinsed with Milli-Q water to remove loosely adsorbed materials. When the material was adsorbed on the surface of the chip, the oscillation frequency decreased. Thus, the adsorption mass per unit area was proportional to the decrease in the resonance frequency, which can be calculated by the Sauerbrey equation

$$\Delta m = -\frac{C\Delta f}{n} \tag{7}$$

where Δf is the vibration frequency of the crystal in Hz, m is the adsorption mass per unit area (mg/m^2), C is the sensitivity factor constant (−0.177 mg·m^{-2}·Hz^{-1}), and n is the number of overtones (N = 3, 5, 7, 9, 11, 13), and the experiment uses the third overtone (15 MHz).

The change in energy dissipation (ΔD) gave relevant information about the viscoelasticity of the adsorption layer

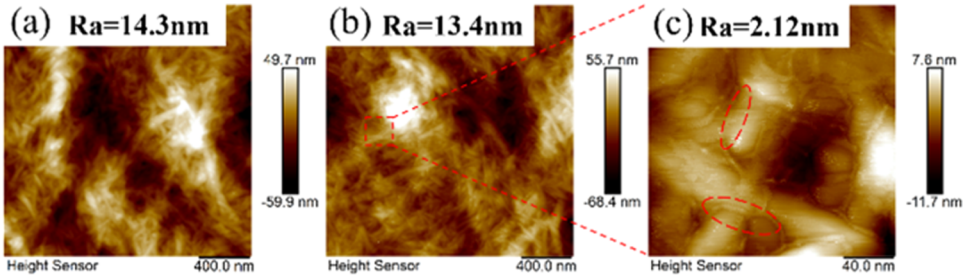

Figure 8. Morphology of the SiO_2 chip with NFC before and after hemicellulose adsorption ((a) NFC covered the SiO_2 chip in the area of 2 × 2 μm^2 and the height scale of 400 nm, (b) hemicellulose adsorbed NFC in the area of 2 × 2 μm^2 and the height scale of 400 nm, and (c) area 200 × 200 nm^2, height scale 40 nm).

https://doi.org/10.1021/acsomega.1c04391
ACS Omega 2021, 6, 30618−30626

$$D = \frac{E_{diss}}{2\pi E_{stored}} \quad (8)$$

where E_{diss} is the energy dissipated in the course of an oscillation and E_{stored} is the total energy stored in the oscillation system.

4.4. AFM Analysis. The morphological characteristics of the cellulose surfaces before and after hemicellulose adsorption were observed using AFM (Bruker Dimension Icon). The tapping mode was used to test the samples collected from the QCM-D experiment with a spring constant of 5 N/m, a probe tip of 2 nm, and a scanning frequency of 1 Hz.

AUTHOR INFORMATION

Corresponding Author

Yang Liu − *School of Light Industry and Food Engineering, Guangxi University, 530004 Nanning, China; Guangxi Key Laboratory of Clean Pulp & Papermaking and Pollution Control, Guangxi University, 530004 Nanning, China; Guangxi Bossco Environmental Protection Technology Co., Ltd., 530000 Nanning, China;* orcid.org/0000-0001-8104-6462; Email: xiaobai@gxu.edu.cn

Authors

Mingzhu Yao − *School of Light Industry and Food Engineering, Guangxi University, 530004 Nanning, China*

Chen Liang − *School of Light Industry and Food Engineering, Guangxi University, 530004 Nanning, China; Guangxi Key Laboratory of Clean Pulp & Papermaking and Pollution Control, Guangxi University, 530004 Nanning, China;* orcid.org/0000-0003-1284-7607

Shuangquan Yao − *School of Light Industry and Food Engineering, Guangxi University, 530004 Nanning, China; Guangxi Key Laboratory of Clean Pulp & Papermaking and Pollution Control, Guangxi University, 530004 Nanning, China;* orcid.org/0000-0003-4982-998X

Hui Zhao − *School of Light Industry and Food Engineering, Guangxi University, 530004 Nanning, China;* orcid.org/0000-0001-8554-9411

Chenni Qin − *School of Light Industry and Food Engineering, Guangxi University, 530004 Nanning, China*

Complete contact information is available at: https://pubs.acs.org/10.1021/acsomega.1c04391

Notes

The authors declare no competing financial interest.

ACKNOWLEDGMENTS

This study was supported by the National Natural Science Foundation of China (NSFC, 22068004) and the Natural Science Foundation of Guangxi, China (2020GXNSFAA159027, 2019GXNSFBA185006, and 2020GXNSFBA159023), Foundation (No. 2019ZR03) of Guangxi Key Laboratory of Clean Pulp & Papermaking and Pollution Control, College of Light Industry and Food Engineering, Guangxi University, and Open Funding Project of the State Key Laboratory of Biocatalysis and Enzyme Engineering (SKLBEE2020009).

ABBREVIATIONS USED

QCM-D:quartz crystal microbalance with dissipation
PEI:polyethylenimine
NFC:nanofibrillated cellulose
BH_{ht}:hemicellulose prepared by the hydrothermal method
BH_{ae}:hemicellulose prepared by alkaline extraction

REFERENCES

(1) Siró, I.; Plackett, D. Microfibrillated cellulose and new nanocomposite materials: a review. *Cellulose* **2010**, *17*, 459−494.
(2) Wang, H.; Li, J. C.; Ding, N.; Zeng, X. H.; Tang, X.; Sun, Y.; Lei, T. Z.; Lin, L. Eco-friendly polymer nanocomposite hydrogel enhanced by cellulose nanocrystal and graphitic-like carbon nitride nanosheet. *Chem. Eng. J.* **2020**, *386*, No. 124021.
(3) Li, C.; Ma, H.; Venkateswaran, S.; Hsiao, B. S. Highly efficient and sustainable carboxylated cellulose filters for removal of cationic dyes/heavy metals ions. *Chem. Eng. J.* **2020**, *389*, No. 123458.
(4) Popp, J.; Kovacs, S.; Olah, J.; Diveki, Z.; Balazs, E. Bioeconomy: Biomass and biomass-based energy supply and demand. *New Biotechnol.* **2021**, *60*, 76−84.
(5) Tang, F.; Yu, H. Y.; Abdalkarim, S. Y. H.; Sun, J. H.; Fan, X. M.; Li, Y. Z.; Zhou, Y.; Tam, K. C. Green acid-free hydrolysis of wasted pomelo peel to produce carboxylated cellulose nanofibers with super absorption/flocculation ability for environmental remediation materials. *Chem. Eng. J.* **2020**, *395*, No. 125070.
(6) Ropitaux, M.; Bernard, S.; Follet-Gueye, M. L.; Vicre, M.; Boulogne, I.; Driouich, A. Xyloglucan and cellulose form molecular cross-bridges connecting root border cells in pea (Pisum sativum). *Plant Physiol. Bioch.* **2019**, *139*, 191−196.
(7) Scheller, H. V.; Ulvskov, P. Hemicelluloses. *Annu. Rev. Plant Biol.* **2010**, *61*, 263−289.
(8) Kim, S.; Kim, K.; Jun, G.; Hwang, W. Wood-Nanotechnology-Based Membrane for the Efficient Purification of Oil-in-Water Emulsions. *ACS Nano* **2020**, *14*, 17233−17240.
(9) Mazeau, K.; Charlier, L. The molecular basis of the adsorption of xylans on cellulose surface. *Cellulose* **2012**, *19*, 337−349.
(10) Escalante, A.; Gonçalves, A.; Bodin, A.; Stepan, A.; Sandström, C.; Toriz, G.; Gatenholm, P. Flexible oxygen barrier films from spruce xylan. *Carbohyd. Polym.* **2012**, *87*, 2381−2387.
(11) Li, Z.; Pan, X. J. Strategies to modify physicochemical properties of hemicelluloses from biorefinery and paper industry for packaging material. *Rev. Environ. Sci. Bio.* **2018**, *17*, 47−69.
(12) Junli, R.; Xinwen, P.; Linxin, Z.; Feng, P.; Runcang, S. Novel hydrophobic hemicelluloses: synthesis and characteristic. *Carbohydr. Polym.* **2012**, *89*, 152−157.
(13) Farhat, W.; Venditti, R. A.; Hubbe, M.; Taha, M.; Becquart, F.; Ayoub, A. A Review of Water-Resistant Hemicellulose-Based Materials: Processing and Applications. *ChemSusChem* **2017**, *10*, 305−323.
(14) Beecher, J. F.; Hunt, C. G.; Zhu, J. Y. Tools for the characterization of biomass at the nanometer scale. In *The Nanoscience and Technology of Renewable Biomaterials*, Lucia, L. A.; Rojas, O. J., Eds.; Academic Press: Wiley-Blackwell: Oxford, UK, 2009; pp 61−90.
(15) Silveira, R. L.; Stoyanov, S. R.; Gusarov, S.; Skaf, M. S.; Kovalenko, A. Plant biomass recalcitrance: effect of hemicellulose composition on nanoscale forces that control cell wall strength. *J. Am. Chem. Soc.* **2013**, *135*, 19048−19051.
(16) Jaafar, Z.; Mazeau, K.; Boissiere, A.; Le Gall, S.; Villares, A.; Vigouroux, J.; Beury, N.; Moreau, C.; Lahaye, M.; Cathala, B. Meaning of xylan acetylation on xylan-cellulose interactions: A quartz crystal microbalance with dissipation (QCM-D) and molecular dynamic study. *Carbohydr. Polym.* **2019**, *226*, No. 115315.
(17) Bosmans, T. J.; Stepan, A. M.; Toriz, G.; Renneckar, S.; Karabulut, E.; Wagberg, L.; Gatenholm, P. Assembly of debranched xylan from solution and on nanocellulosic surfaces. *Biomacromolecules* **2014**, *15*, 924−930.
(18) Köhnke, T.; Ostlund, A.; Brelid, H. Adsorption of arabinoxylan on cellulosic surfaces: influence of degree of substitution and substitution pattern on adsorption characteristics. *Biomacromolecules* **2011**, *12*, 2633−2641.
(19) Linder, Å.; Bergman, R.; Bodin, A.; Gatenholm, P. Mechanism of Assembly of Xylan onto Cellulose Surfaces. *Langmuir* **2003**, *19*, 5072−5077.

(20) Wang, Y.; Zhang, Y.; Zhang, T. C.; Xiang, G.; Wang, X.; Yuan, S. Removal of Trace Arsenite through Simultaneous Photocatalytic Oxidation and Adsorption by Magnetic Fe3O4@PpPDA@TiO2 Core−Shell Nanoparticles. *ACS Appl. Nano Mater.* **2020**, *3*, 8495−8504.
(21) Tammelin, T.; Merta, J.; Johansson, L. S.; Stenius, P. Viscoelastic properties of cationic starch adsorbed on quartz studied by QCM-D. *Langmuir* **2004**, *20*, 10900−10909.
(22) Dalvi, L. C.; Laine, C.; Virtanen, T.; Liitiä, T.; Tenhunen, T.-M.; Orelma, H.; Tammelin, T.; Tamminen, T. Study of xylan and cellulose interactions monitored with solid-state NMR and QCM-D. *Holzforschung* **2020**, *74*, 643−653.
(23) Benselfelt, T.; Cranston, E. D.; Ondaral, S.; Johansson, E.; Brumer, H.; Rutland, M. W.; Wagberg, L. Adsorption of Xyloglucan onto Cellulose Surfaces of Different Morphologies: An Entropy-Driven Process. *Biomacromolecules* **2016**, *17*, 2801−2811.
(24) Lucenius, J.; Parikka, K.; Österberg, M. Nanocomposite films based on cellulose nanofibrils and water-soluble polysaccharides. *React. Funct. Polym.* **2014**, *85*, 167−174.
(25) Villares, A.; Moreau, C.; Dammak, A.; Capron, I.; Cathala, B. Kinetic aspects of the adsorption of xyloglucan onto cellulose nanocrystals. *Soft Matter* **2015**, *11*, 6472−81.
(26) Tammelin, T.; Österberg, M.; Johnsen, I. A. Adsorption of colloidal extractives and dissolved hemicelluloses on thermomechanical pulp fiber components studied by QCM-D. *Nordic Pulp Pap. Res. J.* **2007**, *22*, 93−101.
(27) Ouyang, L.; Zhang, Y.; Wang, Y.; Wang, X.; Yuan, S. Insights into the Adsorption and Photocatalytic Oxidation Behaviors of Boron-Doped TiO_2/g-C3N4 Nanocomposites toward As(III) in Aqueous Solution. *Ind. Eng. Chem. Res.* **2021**, *60*, 7003−7013.
(28) Moser, C.; Backlund, H.; Lindström, M.; Henriksson, G. Xyloglucan for estimating the surface area of cellulose fibers. *Nord. Pulp Pap. Res. J.* **2018**, *33*, 194−199.
(29) Ouyang, L.; Wang, Y.; Zhang, P.; Wang, X.; Yuan, S. Heterostructured MWCNTs@PANI@TiO2 Nanocomposites for Enhanced Adsorption of As(III) from Aqueous Solution: Adsorption and Photocatalytic Oxidation Behaviors. *Ind. Eng. Chem. Res.* **2020**, *59*, 11743−11756.
(30) Zhang, Y.; Wang, X.; Wang, P.; Song, J.; Jin, Y.; Rojas, O. J. Interactions between type A carbohydrate binding modules and cellulose studied with a quartz crystal microbalance with dissipation monitoring. *Cellulose* **2020**, *27*, 3661−3675.
(31) Naidjonoka, P.; Hernandez, M. A.; Palsson, G. K.; Heinrich, F.; Stalbrand, H.; Nylander, T. On the interaction of softwood hemicellulose with cellulose surfaces in relation to molecular structure and physicochemical properties of hemicellulose. *Soft Matter* **2020**, *16*, 7063−7076.
(32) Lopez, M.; Bizot, H.; Chambat, G.; Marais, M. F.; Zykwinska, A.; Ralet, M. C.; Driguez, H.; Buleon, A. Enthalpic studies of xyloglucan-cellulose interactions. *Biomacromolecules* **2010**, *11*, 1417−1428.
(33) Lucenius, J.; Valle-Delgado, J. J.; Parikka, K.; Osterberg, M. Understanding hemicellulose-cellulose interactions in cellulose nanofibril-based composites. *J. Colloid. Interface Sci.* **2019**, *555*, 104−114.
(34) Wang, Y.; Zhang, P.; Zhang, T. C.; Xiang, G.; Wang, X.; Pehkonen, S.; Yuan, S. A magnetic γ-Fe_2O_3@PANI@TiO_2 core−shell nanocomposite for arsenic removal via a coupled visible-light-induced photocatalytic oxidation−adsorption process. *Nanoscale Adv.* **2020**, *2*, 2018−2024.
(35) Aulin, C.; Varga, I.; Claesson, P. M.; Wagberg, L.; Lindstrom, T. Buildup of polyelectrolyte multilayers of polyethyleneimine and microfibrillated cellulose studied by in situ dual-polarization interferometry and quartz crystal microbalance with dissipation. *Langmuir* **2008**, *24*, 2509−2518.
(36) Zhang, Y.; Jiang, D.; Wang, Y.; Zhang, T. C.; Xiang, G.; Zhang, Y.-X.; Yuan, S. Core−Shell Structured Magnetic γ-Fe_2O_3@PANI Nanocomposites for Enhanced As(V) Adsorption. *Ind. Eng. Chem. Res.* **2020**, *59*, 7554−7563.
(37) Pereira, C. S.; Silveira, R. L.; Dupree, P.; Skaf, M. S. Effects of Xylan Side-Chain Substitutions on Xylan-Cellulose Interactions and Implications for Thermal Pretreatment of Cellulosic Biomass. *Biomacromolecules* **2017**, *18*, 1311−1321.

https://doi.org/10.1021/acsomega.1c04391
ACS Omega 2021, 6, 30618−30626